DOI: 10.12442/j.issn.1002-185X.20240100

Effects of thermal aging on interface microstructure and mechanical properties of hot isostatic pressing densified Inconel 690 cladding on low alloy steel

Lei Yu[1,2], Rui Cao[1,2], Jinyuan Ma[1,2], Yingjie Yan[1,2], Hao Dong[3,4], Caiqin Wang[3,4]

[1] State Key Laboratory of Advanced Processing and Recycling of Non-ferrous Metal, Lanzhou University of Technology, Lanzhou 730050, China; [2] School of Materials Science and Engineering, Lanzhou University of Technology, Lanzhou 730050, China; [3] Advanced Technology & Materials Co., Ltd., Beijing 100081, China; [4] Hebei Hot Isostatic Pressing Technology Innovation Center, Zhuozhou 072750, China

Abstract: The interface microstructure, micro-hardness, and tensile properties of hot isostatic pressing (HIP) densified Inconel 690 cladding on low alloy steel were investigated during the 600℃-aging process. The interface region can be divided into four zones - carbon-depleted zone (CDZ), partial melting zone (PMZ), planar growth zone (PGZ), and brownish feature zone (BFZ) - from base metal to deposited metal. Dimensions of these zones do not significantly change during aging. However, type I carbides noticeably increase in size in the PMZ, and precipitates clearly occur in the PGZ. The main reason for their growth and occurrence is continuous carbon migration. Micro-hardness of the interface shows that the highest hardness appears in the PGZ and BFZ region, which is related to carbon accumulation and precipitates in this region. Tensile failure occurs on the base metal side due to the high strength mismatch between these two materials and is located at the boundary of CDZ and base metal due to the lower strength of only ferrite. The ultimate tensile strength decreases by only 50 MPa after aging for 1500 h, and the interface region maintains high strength with no significant deformation.

Key words: interface; thermal aging; microstructure; mechanical properties; hot isostatic pressing densification

Claddings of Ni-based alloys on steel are usually used in oil, petrochemical, nuclear, and marine industries, owing to their excellent wear, corrosion, and high-temperature oxidation resistance[1-4]. High-quality claddings are commonly required for long-term security service. However, Ni-based alloys are easily suffering from welding defects, like solidification cracking[5-6], liquid cracking[6-7], ductility-dip cracking[8-9], strain-age cracking[10], and pores[11]. To reduce these defects, various methods have been developed, including welding method optimization[12-13], welding and heat treatment parameter adjustment[14-15], rare earth element addition[16], and hot isostatic pressing (HIP) densification[17].

HIP densification has been proven to be an effective method for healing welding defects in Ni-based alloys[18]. However, most studies have focused on densification parameters and degrees[17-20], with few studies have investigated interface evolution, especially for interface microstructure and mechanical properties evolution in a thermal environment. Ni-based alloy/steel interfaces have complex microstructures and are prone to premature failure. Zhang Y[21] showed that the formation and propagation of oxide resulted in interfacial failure of the Inconel 617/9Cr steel under creep conditions. Choi KJ[22] found that Cr carbides were enhanced by thermal aging near the interface. They also found that galvanic corrosion occurred near the interface of both Alloy 152/low alloy steel and Alloy 182/low alloy steel[23]. Kim J[24] determined that thermal aging creates a susceptibility to stress corrosion cracking of Ni-based alloy/low alloy steel interface. Therefore, a fundamental understanding of the unique microstructure and mechanical properties of interface is required to improve the understanding of the degradation and failure behaviors.

Microstructure and mechanical properties are key parameters affecting materials degradation and failure. Also, accelerated thermal aging is required to investigate the thermal aging

Received date:
Foundation item: Major Scientific and Technological Project of Gansu (No. 22ZD6GA008); Excellent Doctorate Project of Gansu (No. 23JRRA806); National Natural Science Foundation of China (Nos. 52175325, 51961024，52071170)
Corresponding author: Rui Cao, Ph.D., Professor, School of Materials Science and Engineering, Lanzhou University of Technology, Lanzhou 730050, P. R. China, Tel: 13893468800, E-mail: caorui@lut.edu.cn

effect on the interface[22]. To investigate the effect of thermal aging on Ni-based alloy/low alloy steel integrity, the current study aims to analyze the microstructure and mechanical properties evolution of the interface between Inconel 690 and low alloy steel of HIP densified and thermally aged using optical microscopy (OM), scanning electron microscopy (SEM), micro-hardness, and tensile test.

1 Experiment

Fig.1 illustrates the schematic of Inconel 690 cladding preparation and subsequent treatment. In this study, 30-mm-thick Q345B low alloy steel was used as the base metal. 1-mm-diameter Inconel 690 wire was used as the deposited metal. The nominal chemical compositions are provided in Table 1. The surface of the base metal was first ground to remove the oxide layer and then cleaned sequentially with acetone, alcohol, and other organic solvents.

Table 1 Chemical composition of deposited metal and base metal (wt %)

Elements	Cr	Fe	Ni	Si	Ti	Al	Mn	C
Inconel 690	27.41	9.50	Bal.	0.19	0.38	0.69	0.72	0.06
Low alloy steel	0.022	Bal.	0.01	0.22	0.0008	0.012	1.21	0.16

The cladding was performed using gas tungsten arc welding to create a layer with a minimum thickness of 15 mm. The overlap ratio for each pass was approximately 30%, and all subsequent passes were conducted at an inter-pass temperature of 170 ℃. Specific welding parameters are listed in Table 2.

Table 1 Chemical composition of deposited metal and base metal (wt %)

Current (A)	Wire feed rate (cm/min)	Welding speed (cm/min)	Gas flow rate (L/min)	Wire feed angle (°)
160	100	15	15	70-75

No post-weld heat treatment was performed after the cladding process. The cladding component was then subjected to HIP densification at a temperature of 1120 ℃, an argon pressure of 150 MPa for 2 h, and cooled in a furnace.

To investigate the evolution of microstructure and mechanical properties of the interface under thermal conditions, some HIP-densified specimens were subjected to thermal aging treatment at a temperature of 600 ℃ (below the phase transition temperature of low alloy steel) for an aging time ranging from 0 h to 1500 h. Specimens aged for 100 h, 200 h, 500 h, 1000 h and 1500 h were selected to analyze the evolution in microstructure, micro-hardness and tensile properties.

The joint was ground with 600-, 800-, 1000-, 1500-, 2000-, and 3000-grid sand papers and polished with diamond particles of 0.25 μm, and then some of the specimens were electrolytically etched by 10 % chromic acid solution to observe the microstructure of the deposited metal. While others were etched by 4 % nital to reveal the microstructure of the base metal. Microstructural characteristics were investigated by OM and SEM fitted with an energy-dispersive spectroscope (EDS).

Micro-hardness and tensile tests were conducted to evaluate the mechanical properties evolution of the joint during aging. The experimental conditions for micro-hardness were as follows: a PG-2 type micro-hardness testing machine was used, with a force of 10N applied for 15s. To ensure reliable results, 10 tests were performed for each specimen along the fusion boundary. The reported hardness was obtained by averaging the results measured at surface displacements of 200 μm for each indentation. The tensile tests were carried out using a universal testing machine at a speed of 0.008 mm/s. Because the thickness of the cladding layer was only 13 mm, the non-standard tensile specimens were machined and their schematic diagram is shown in Fig. 1.

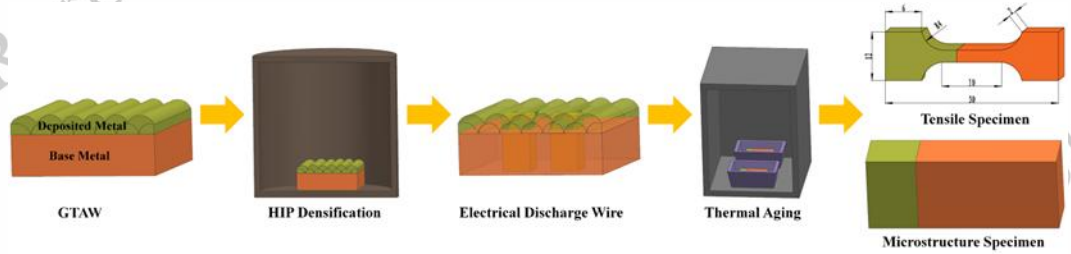

Fig. 1. Schematic of Inconel 690 cladding preparation and subsequent treatment (unit: mm).

2 Results and Discussion

2.1 Microstructure of the HIP densified interface

Fig. 2(a) shows a macroscopic OM micrograph of the HIP-densified interface on the base metal side. The microstructure far away from the fusion boundary consists of typical ferrite and pearlite, while the microstructure close to the fusion boundary is composed of ferrite with a grain size of several tens of microns. This result is caused by cementite dissolution at about 500 μm from the fusion boundary and carbon diffusion from the base metal to the deposited metal. Hence, this region is sometimes referred to as the carbon-depleted

zone (CDZ) or decarburized zone[25-27].

Fig. 2(b) displays a macroscopic OM micrograph of the HIP densified interface on the deposited metal side. The bottom of the first welding layer and the second layer mainly exhibits cellular dendrites with large elongated grains, which are millimeter-sized in the welding solidification direction, and several hundred microns wide in the transversal section. Meanwhile, the surface of the first welding layer and the second layer mainly exhibits equiaxed structures with several hundred microns grains.

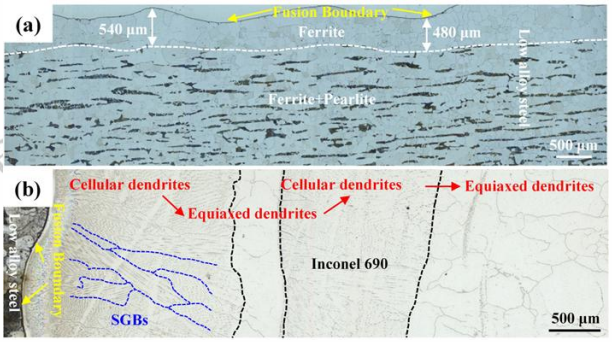

Fig.2. Macroscopic OM micrograph of the HIP-densified interface (SGBs-solidification grain boundaries). (a) base metal; (b) deposited metal.

To investigate the interface microstructure in detail, a high magnification OM micrograph was analyzed, as shown in Fig. 3(a). A white layer of about 10 μm without any obvious features is revealed, and it exhibits planar grains. After that, the grains changed to cellular grains far away from the fusion boundary. This is related to the change of its solidification modes during welding and is controlled by temperature gradient in the liquid (G_L), solidification growth rate (R), and composition[28]. Heterogeneous nucleation off a solid substrate is called epitaxial nucleation. When the compositions of the substrate and liquid are similar, the solidification front that grows from a given grain on that substrate will retain the same crystallographic orientation. Since grain orientation of the substrate is generally random, this results in a continuation of the crystallographic misorientation of the base metal grains across the fusion boundary into the solidifying solid. That is to say, grain boundaries are continuous across the original fusion boundary where epitaxial nucleation occurred. In fcc and bcc metals, solidification growth occurs preferentially along the cube edge, or <100> crystallographic directions. These are sometimes called “easy growth” directions, since solidification is most efficient in this crystallographic orientation, as shown in Fig. 3(b)[28-30].

Fig. 4 shows SEM micrograph and corresponding EDS result of the HIP densified interface. The interface from base metal to deposited metal can be divided into carbon-depleted zone (CDZ), partial melting zone (PMZ), and partially mixed zone. The CDZ is composed of ferrite according to the OM micrograph analysis in Fig. 1. The PMZ is the actual fusion boundary in Fig. 1 and is about 5 μm wide in Fig. 4(a). From the magnified micrograph and the EDS result of this region, as shown in Fig. 5, it is clear that the PMZ is rich in carbon content compared to that of the CDZ and the PGZ, and has the morphology of type I and type II carbides, which are commonly reported in Ni-based alloy/steel interface after high temperature long-term service[31-33]. The partially mixed zone is divided into two zones according to the SEM morphology in this study, namely planar growth zone (PGZ) and brownish feature zone (BFZ). These two zones are separated by planar grain boundaries. The PGZ appears as a bright band of about 10 μm in Fig. 3(a) and has no distinct feature in Fig. 4(a). The BFZ reveals such a difference with the PGZ in Fig. 4(a) and is located at the deposited metal side adjacent to the PGZ. According to the research of LAS/Alloy 52 by Akhatova A[27], nano-sized $M_{23}C_6$ precipitates were observed in the BFZ, and no thermodynamically predicted Cr_7C_3 carbides were found in the PGZ. This can primarily explain the difference in morphology between the PGZ and the BFZ in Fig. 4(a). As usually observed in interface and consistent with the compositions given in Table 1, a compositional gradient exists between the base metal and deposited metal. Fig. 4(b) shows a distinct intermediate zone with substitutional content gradients, characteristic of a compositional transition region. Fe, Ni, and Cr contents change gradually across the PMZ, PGZ, and BFZ, and the transition distance is about 20 μm.

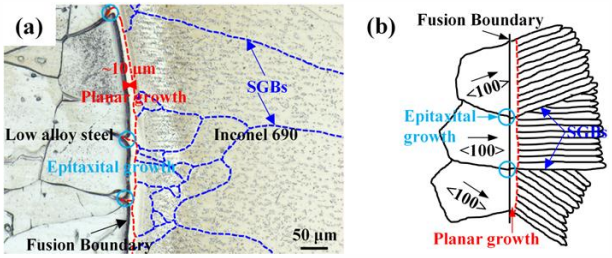

Fig. 3. (a) High magnification OM micrograph of the interface region (red line- the boundary of the planar growth; blue lines- SGBs; light blue circles- epitaxial growth). (b) Schematic of the epitaxial nucleation mechanism [28].

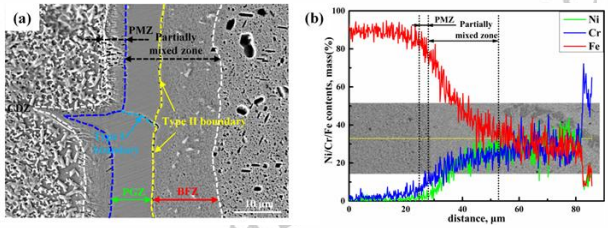

Fig. 4. (a) Interface region SEM micrograph of the HIP-densified interface (PMZ-partially melted zone, PGZ-planar growth zone, BFZ- brownish feature zone). (b) EDS line scanning results of Ni, Cr and Fe around the interface region.

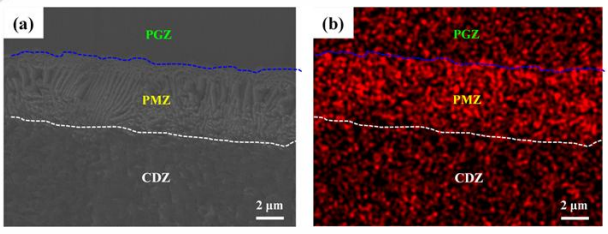

Fig. 5. SEM micrograph and corresponding carbon content of the HIP-densified interface (CDZ- carbon-depleted zone).

2.2 Evolution of microstructure during aging

The joint was subjected to thermal aging for 100h, 200h, 500h, 1000h and 1500h, respectively. The microstructure of the interface was analyzed by SEM, as shown in Fig. 6. The PMZ, PGZ and BFZ were observed to have dimensions similar to those observed in Fig. 4(a), with no obvious change during the aging process. However, morphologies of the PMZ and the PGZ after aging show significant differences when compared to the HIP densified, especially after aging 1500h, as shown in Fig. 7(a). Larger type I carbides appear in the PMZ, with a slight increase in width of about 1-2 μm. In Fig. 7(b), needle-shaped precipitates occur in the PGZ, which are not present in the HIP densified. This phenomenon may be attributed to carbon migration and carbide precipitation during the aging process.

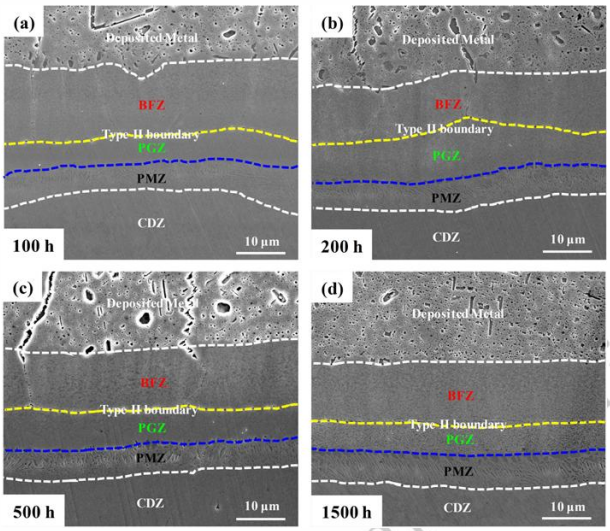

Fig. 6. Interface region SEM micrographs of the interface during the aging process. (a) 100h, (b) 200h, (c) 500h, (d) 1500h

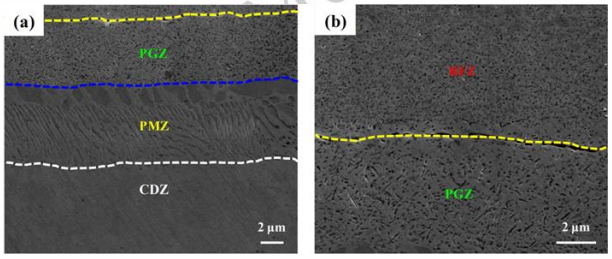

Fig. 7. Interface region SEM micrographs of the interface after aging 1500h. (a) PMZ and PGZ. (b) PGZ and BFZ.

2.3 Evolution of mechanical properties during aging

To evaluate the mechanical properties evolution of the joint during the aging process, the micro-hardness and tensile properties of the joint were examined. Fig. 8 illustrates the micro-hardness evolution of the interface region during aging. The higher micro-hardness appears at the deposited metal side. No significant difference occurs between the HIP densified and aged except for the first point of the deposited metal. The first point of the deposited metal has the highest micro-hardness and is located in the region between PGZ and BFZ, as observed in Fig. 8(a). The micro-hardness of this region changes much more than that of other regions. After 100h, the micro-hardness increases from 380.3 HV to 473.4 HV and remains essentially constant during aging for 200h, 500h, and 1000h. The micro-hardness reaches 518.8 HV after aging for 1500h, which is the highest value obtained in this work, as shown in Fig. 8(b).

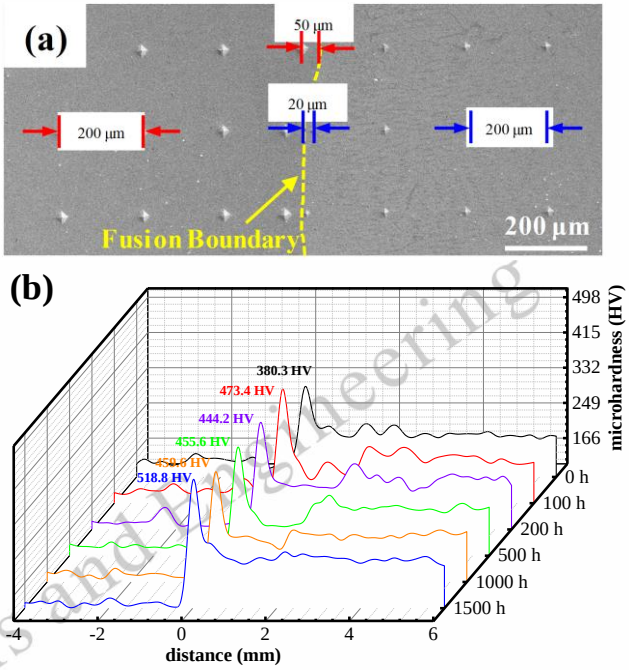

Fig. 8. Micro-hardness of HIP densified and aged interface. (a) Location of indentations in the interface region, (b) Micro-hardness evolution during aging.

Fig. 9 illustrates the evolution of ultimate tensile strength of the joint. It is observed that the strength slightly decreases with aging time, and after aging for 1500h, it was about 50 MPa lower than that of the HIP densified specimens. The failure occurred on the base metal side, exhibiting obvious plastic deformation as shown in the insert in Fig. 10. Fig. 10 demonstrates the evolution of the interface region after tensile. No significant plastic deformation was observed on the deposited metal side for all specimens. However, serious deformation occurs on the base metal side along the interface. This phenomenon indicates that the deposited metal did not reach the yield stress during tensile. The large strength difference between the deposited metal and the base metal leads to yield first in the base metal. Meanwhile, The CDZ is composed of only ferrite, rather than ferrite and pearlite for the base metal. These two reasons cause necking to occur at the boundary between CDZ and base metal. The 50 MPa decrease in strength means aging has small influence on the tensile strength, and the interface still has a higher strength compared to the base metal.

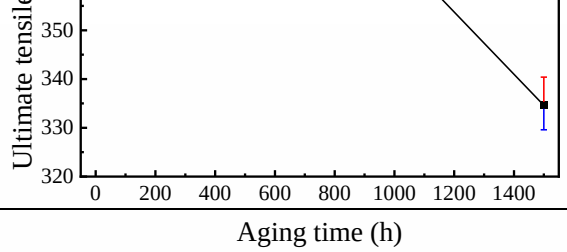

Fig. 9. Ultimate tensile strength evolution of the joint during aging process.

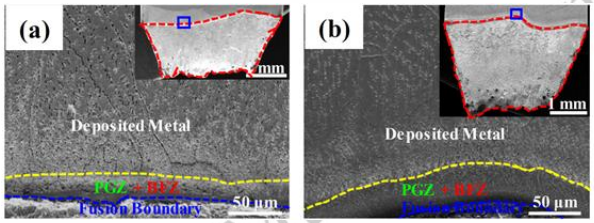

Fig. 10. SEM micrograph of the interface region after tensile test (The inset shows macroscopic morphology of fracture profile). (a) HIP densified; (b) 1500h aged.

2.4 Interface microstructure evolution during aging

The interface region can be classified into four distinct zones from the base metal to the deposited metal, which are CDZ, PMZ, PGZ, and BFZ. The PMZ is identified as fusion boundary in OM images (Fig. 1, Fig. 2, and Fig. 3) due to low magnification, and reveals a 5-8 μm wide band rich in carbon content with type I and/or type II carbide morphology in SEM images (Fig. 4, Fig. 5, Fig. 6, and Fig. 7). SEM and EDS results in Fig. 5 show that lath type II carbides with a high carbon content clearly appears in the PMZ. After aging 1500h, carbides, particularly the spheroidicity type I carbides, significantly grow, as shown in Fig. 7(a). These results are consistent with Parker's research that type I carbides grow with aging time at 625°C[31]. The PGZ with 10 μm wide is adjacent to the fusion boundary, it is also referred to as "featureless zone" by Dai T and Lippold J C[34, 35]. This zone has no obvious precipitates in the HIP densified condition, as shown in Fig. 4(a). However, after aging, evident needle-shaped M_7C_3 carbides appear in this zone, as per Dodge's researches[36, 37]. The BFZ is part of the deposited metal cellular grains adjacent to the PGZ, and this zone exhibits a clear difference in precipitates from the deposited metal, as shown in Fig. 6. TEM results have confirmed that the precipitates in the BFZ are nano-sized $M_{23}C_6$ carbides[27].

Based on the microstructure observation of the interface region, the bonding between the base metal and the deposited metal is attributed to the epitaxial growth mechanism. The melted weld metal nucleates along the grain boundaries of base metal and rapidly solidifies into planar crystals during the welding solidification process. As a result of quick solidification, the precipitated phase does not have enough time to form, resulting in the "featureless zone". After planar growth, the solidification rate decreases but remains high, resulting in the formation of BFZ, where nano-sized $M_{23}C_6$ precipitates form. As the solidification rate continues to decrease, larger precipitates form in the cellular grains. Carbides in the PGZ and BFZ increase after aging, particularly in the PGZ after aging for 1500h. It is attributed to the aging temperature promoting carbon migration from the base metal to the deposited metal, resulting in high carbon solution at high temperature. After the aging process, the temperature gradually decreases, and the carbon solution also decreases, leading to the precipitation of M_7C_3 and $M_{23}C_6$ carbides in the PGZ and the BFZ, respectively.

2.5 Properties evolution of the interface region

The PGZ and BFZ region exhibits the highest micro-hardness value, which is consistent with previous studies[12, 34, 38]. The micro-hardness of this region increases from 380.3 HV to 473.4 HV after 100h of aging and remains nearly constant for 200h, 500h, and 1000h, indicating that precipitates have already precipitated in this region and the balance between the number and size of precipitates results in the stable micro-hardness in subsequent processes. After aging for 1500h, the micro-hardness increases significantly to 518.8 HV due to continuous carbon migration and a greater number of precipitates in the PGZ and BFZ, as reported by other studies[15, 27, 35-37].

Tensile tests show that the interface region was not the weakest zone. The failure occurs on the base metal side with significant plastic deformation. In contrast, after tensile no obvious deformation is produced at the deposited metal side, including the PGZ and the BFZ, indicating higher yield stress compared to the base metal. During the tensile process, yield phenomena first appears at the base metal, while the deposited metal is remained in the elastic process. The deformation hardening of the base metal could not reach the yield stress of the deposited metal, indicating a high strength mismatch between these two materials. As a result, the deformation is concentrated at the base metal side and ultimately fractured from the weakest zone. The CDZ, composed of only ferrite rather than ferrite and pearlite of the base metal, has lower strength and fractures at the boundary between CDZ and base metal. The strength only decreases by 50 MPa after 1500h, indicating aging has little influence on the tensile strength of the joint.

3 Conclusions

1) Interface of the joint can be divided into CDZ, PMZ, PGZ, and BFZ zones from the base metal to the deposited metal. Due to carbon migration and cementite dissolution, the CDZ reveals only ferrite rather than ferrite and pearlite in the base metal, and the grain size is obviously larger than that of the base metal. The PMZ shows a band of about 5-8 μm with type I and/or type II carbides. The PGZ shows a 10 μm epitaxial growth band from the PMZ, which has featureless for the HIP densification specimen. However, obvious precipitates occur after thermal aging. The BFZ is part of the deposited metal cellular grains adjacent to the PGZ, with much smaller precipitates than that of the deposited metal.

2) The continuous carbon migration and more precipitates in PGZ and BFZ resulted in higher micro-hardness, which increased from 380.4 HV to 518.8 HV after aging 1500h.

3) Tensile strength of the joint is slightly decreased by 50 MPa after aging, and fractures are all located in the base metal. The huge difference between the two materials leads to the base metal yield firstly, and subsequent deformation hardening also can not reach the yield strength of the deposited metal.

Cementite dissolves in the CDZ leading to this zone having the lowest strength and resulting in fracture at the boundary of the CDZ and the base metal.

References

1 Huang J, Liu S, Yu S *et al. Journal of Manufacturing Processes*[J], 2020, 56: 106

2 [2] Liu Q, Liu Z, Wang Y *et al. Rare Metal Materials and Engineering*[J], 2023, 52(04): 1210

3 Zareie Rajani H R, Akbari Mousavi S A A. *Journal of Failure Analysis and Prevention*[J], 2012, 12: 646

4 Zareie Rajani H R, Akbari Mousavi S A A. *Materials Science and Engineering: A*[J], 2012, 556: 454

5 Wang D, Kadoi K, Yamamoto M *et al. Rare Metal Materials and Engineering*[J], 2021, 50(7): 2435

6 Guo Y, Zhang J, Xiong J *et al. Rare Metal Materials and Engineering*[J], 2021, 50(4): 1462

7 Aqeel M, Shariff S M, Gautam J P *et al. Materials and Manufacturing Processes*[J], 2021, 36: 904

8 Rapetti A, Christien F, Tancret F *et al. Scripta Materialia*, 2021, 194: 113680

9 Chen J, Zhang P, Mo T *et al. Science and Technology of Welding and Joining*[J], 2021, 26(4): 294

10 Zhang G, Xiao C, Taheri M. *Journal of Manufacturing Processes*[J], 2020, 52: 66

11 Chiang M F, Chen C. *Materials Chemistry and Physics*[J], 2009, 114: 415

12 Ming H, Zhang Z, Wang J *et al. Materials Characterization*[J], 2017, 123:233

13 Frei J, Alexandrov B T, Rethmeier M. *Welding in the World*[J], 2018, 62:317

14 Xu F J, Lv Y H, Xu B S *et al. Materials & Design*[J], 2013, 45: 446-

15 Liu F C, Nelson T W, McCracken S L. *Metallurgical and Materials Transactions A*[J], 2019, 50(6): 2826

16 Saida K, Taniguchi A, Okauchi H *et al. Science and Technology of Welding and Joining*[J], 2013, 16(6): 553

17 Hsu K T, Wang H S, Chen H G *et al. Metals*[J], 2016, 6(10): 238

18 Xie J, Ma Y, Xing W *et al. Welding in the World*[J], 2018, 62: 471

19 Sentyurina Z A, Baskov F A, Loginov P A *et al. Additive Manufacturing*[J], 2021, 37: 101629

20 Tillmann W, Schaak C, Nellesen J *et al. Additive Manufacturing*[J], 2017, 13: 93

21 Zhang Y, Li K, Cai Z *et al. Materials Science and Engineering: A*[J], 2019, 764: 138185

22 Choi K J, Kim J J, Lee B H *et al. Journal of Nuclear Materials*[J], 2013, 441: 493

23 Choi K J, Yoo S C, Kim S *et al. Corrosion Science*[J], 2019, 153: 138

24 Kim J, Kim S H, Choi K J *et al. Corrosion Science*[J], 2014, 86: 295

25 Lindqvist S, Ahonen M, Lydman J *et al. Engineering Fracture Mechanics*[J], 2019, 214: 320

26 Ming H, Zhang Z, Wang J *et al. Materials Characterization*[J], 2019, 148: 100

27 Akhatova A, Robaut F, Verdier M *et al. Materials Science and Engineering: A*[J], 2020, 788: 139592

28 Lippold J C. Welding Metallurgy Principles, Welding metallurgy and weldability[M]. *New York: John Wiley & Sons*, 2014: 9

29 Ranjbar K, Dehmolaei R, Amra M *et al. Welding in the World*[J], 2018, 62(6): 1121

30 Devendranath Ramkumar K, Arivazhagan N, Narayanan S. *Materials & Design*[J], 2012, 40: 70

31 Parker J D, Stratford G C. *Journal of Materials Science*[J], 2000, 35: 4099

32 Nicholso R D. *Metals Technology*[J], 1984, 11: 115

33 Li K J, Li X G, Zhang Y *et al. Electric Welding Machine*[J], 2020, 50(9): 17 (in Chinese)

34 Dai T, Lippold J C. *Journal of Materials Engineering and Performance*[J], 2018, 27(7): 3411-3418

35 Dai T, Lippold J C. *Welding in the World*[J], 2018, 62(3): 535

36 Dodge M F, Dong H B, Gittos M F. *Materials Research Innovations*[J], 2014, 18(sup4): S4-907

37 Dodge M F. The effect of heat treatment on the embrittlement of dissimilar welded joints[D]. *Leicester: University of Leicester*, 2014

38 Dong L, Peng Q, Xue H *et al. Corrosion Science*[J], 2018, 132: 9

时效对热等静压致密化低合金钢上堆焊 Inconel 690 界面组织及性能的影响

余磊[1,2]，曹睿[1,2]，马金元[1,2]，闫英杰[1,2]，董浩[3,4]，王彩芹[3,4]

(1. 兰州理工大学 省部共建有色金属先进加工与再利用国家重点实验室，甘肃 兰州 730050)

(2. 兰州理工大学 材料科学与工程学院，甘肃 兰州 730050)

(3. 安泰科技股份有限公司，北京 100081)

(4. 河北热等静压技术创新中心，河北 涿州 072750)

摘　要：在600℃时效处理过程中，对热等静压（HIP）致密化处理的低合金钢上堆焊Inconel 690界面微观结构、微硬度和拉伸性能进行了研究。从基体到堆焊层，界面区域可以分为四个区域 - 贫碳区（CDZ）、局部熔化区（PMZ）、平面生长区（PGZ）和棕色特征区（BFZ）。这些区域的尺寸在时效过程中没有显著变化。然而，I型碳化物在PMZ中明显增大，而在PGZ中明显出现沉淀。它们长大和出现的主要原因是时效过程中连续的碳迁移。界面最高硬度出现在PGZ和BFZ区域，这与该区域中碳的堆积和沉淀有关。由于这两种材料之间高的强度不匹配性，拉伸失效发生在基体侧，并且由于仅有铁素体组织，位于CDZ和基体的界面处。在经过1500小时的时效处理后，抗拉强度仅降低了50 MPa，并且界面区域保持高强度且无明显变形。

关键词：界面；时效；组织；机械性能；热等静压致密化

作者简介：曹睿，女，博士，教授，材料科学与工程学院，兰州理工大学，甘肃 兰州 730050，电话：13893468800，E-mail: caorui@lut.edu.cn